Design and Development of a Handheld Haptic Device for Force and Stretch Feedback in Virtual Environments

by

Berke Ataseven

A Dissertation Submitted to the
Graduate School of Sciences and Engineering
in Partial Fulfillment of the Requirements for
the Degree of

Master of Science

in

Mechanical Engineering

KOÇ ÜNİVERSİTESİ

March 2, 2023

Design and Development of a Handheld Haptic Device for Force and Stretch Feedback in Virtual Environments

Koç University

Graduate School of Sciences and Engineering

This is to certify that I have examined this copy of a master's thesis by

Berke Ataseven

and have found that it is complete and satisfactory in all respects,
and that any and all revisions required by the final
examining committee have been made.

Committee Members:

_____

Prof. Dr. Çağatay Başdoğan (Advisor)

_____

Assist. Prof. Mine Saraç Stroppa

_____

Assoc. Prof. Asım Evren Yantaç

Date: _____

To friends and family whose love and support were never missing in my hardest times. I would not have done it without you.

ABSTRACT

Design and Development of a Handheld Haptic Device for Force and Stretch Feedback in Virtual Environments
Berke Ataseven
Master of Science in Mechanical Engineering
March 2, 2023

This thesis presents the design and development of a handheld haptic device capable of delivering force feedback to users for grasping and squeezing virtual objects and also stretch feedback for rendering inertial effects in virtual environments. The device utilizes cable-driven mechanisms and is equipped with four force sensors and two DC motors. The design and development process involved evaluating various mechanical and electronic components, selecting the proper ones and assembling them, and conducting user studies to assess the effectiveness of the device in virtual environments.

The user studies conducted for evaluating the force feedback feature of the device demonstrated that the range of object stiffness that can be effectively conveyed to users in virtual environments can be significantly expanded by controlling the relationship between visual and haptic cues. We propose that a single variable, named Apparent Stiffness Difference, can predict the pattern of human stiffness perception under manipulated conflict, which can be used for rendering a range of soft objects in VEs larger than what is achievable by a haptic device alone due to its physical limits.

The results of our user studies conducted for evaluating the palm stretch feedback feature of the device showed that both the tactor displacement and speed play a significant role in the perceived intensity of skin stretch. The mapping between these two factors was found to be nonlinear. Additionally, the results showed that the tactile sensitivity of the human palm to skin stretch applied by a tactor is uniform; stretch applied to the radial direction (towards the thumb) results in a similar intensity to that of the ulnar direction (away from the thumb).

ÖZETÇE

Sanal Ortamlarda Kuvvet ve Esneme Geri Bildirimi için El Tipi Haptik Cihaz Tasarımı ve Geliştirilmesi

Berke Ataseven

Makine Mühendisliği, Yüksek Lisans

2 Mart 2023

Bu tez, sanal nesneleri kavramak ve sıkmak için kullanıcıların işaret ve baş parmaklarına kuvvet geri bildirimi sağlayan ve ayrıca sanal ortamlarda atalet efektleri oluşturmak için kullanıcının avuç içine gerilme geri bildirimi sağlayan bir haptik cihazın tasarımını ve geliştirilmesini sunmaktadır. Cihaz kablo tahrikli mekanizmalar kullanmaktadır ve dört kuvvet sensörü ve iki DC motor ile donatılmıştır. Tasarım ve geliştirme süreci, çeşitli mekanik ve elektronik bileşenlerin değerlendirilmesini, uygun olanların seçilmesini ve monte edilmesini ve cihazın sanal ortamlardaki etkinliğini değerlendirmek için kullanıcı çalışmaları yapılmasını içermektedir.

Cihazın kuvvet geribildirimi özelliğini değerlendirmek için yapılan kullanıcı çalışmaları, sanal ortamlarda kullanıcılara etkili bir şekilde iletilebilen nesne sertliği aralığının, görsel ve dokunsal ipuçları arasındaki ilişki kontrol edilerek önemli ölçüde genişletilebileceğini göstermiştir. "Görünür Sertlik Farkı" olarak adlandırılan tek bir değişkenin, manipüle edilmiş çatışma altında insan sertlik algısını tahmin edebileceğini gösteriyoruz.

Cihazın avuç içi esneme geribildirimi özelliğini değerlendirmek için yürüttüğümüz kullanıcı çalışmalarının sonuçları, deri esnemesinin dokunsal algı yoğunluğunda hem dokunaç yer değiştirmesinin hem de hızının önemli bir rol oynadığını göstermiştir. Bu iki faktör arasındaki eşleşmenin doğrusal olmadığı tespit edilmiştir. Ayrıca sonuçlar, insan avucunun bir dokunaç tarafından uygulanan deri gerilmesine karşı dokunsal hassasiyetinin homojen olduğunu; radyal yöne (başparmağa doğru) uygulanan gerilmenin ulnar yöndekine (başparmaktan uzağa) benzer bir yoğunlukla algılandığını göstermiştir.

TABLE OF CONTENTS

List of Tables viii

List of Figures ix

Abbreviations xiii

Chapter 1: Introduction 1

Chapter 2: Design of The Handheld Haptic Device 7

2.1 Grasper with Force Feedback 7

2.1.1 Force Tracking 7

2.2 Handle with Stretch Feedback 9

2.3 Controller Board 11

2.4 Earlier Designs 13

Chapter 3: Experiments 16

3.1 Force Feedback Experiments 16

3.2 Stretch Feedback Experiments 20

Chapter 4: Results 21

4.1 Results of Force Feedback Experiments 21

4.2 Results of Stretch Feedback Experiments 26

Chapter 5: Discussion 29

Chapter 6: Conclusion 30

Bibliography 32

Appendix A: Haptic Device Interface **38**

LIST OF TABLES

4.1 Coefficients of the proposed model. 28

LIST OF FIGURES

2.1 Internal structure of our handheld haptic device and the close-up view of the thimbles. The electric motor inside the handle (not shown) rotates and translates the thimbles in accordance with the forces applied by the index finger and thumb, which are measured by the pressure sensors attached to the inner walls of the thimbles. This allows a resistance-free movement of the fingers when there is no contact with the virtual object and renders its stiffness when there is. For easy fit to fingers and comfortable use of the device, the thimbles can passively rotate around the vertical axis shown in the close-up view. 8

2.2 The motor actuates and moves the sliders to match the applied user force (measured by the FSR sensors) with the desired force. Note that the positive and negative values of user force are the sum of the forces read from the FSR sensors on the inner and outer walls of the thimbles, respectively. a) Desired force is equal to zero when there is no contact with the virtual object. b) The user and desired forces are shown as the user repetitively squeezes the virtual object. The desired force changes as the user moves their fingers while holding the object. The user force lags behind the desired force, and the force controller aims to compensate for the lag by adjusting the motor speed. 9

2.3 Back view of the haptic device with one of the half cylinders of the handle displayed transparently to show the device's internals. Cable-driven mechanism translates the rotation of the motor shaft into the translational motion of the tactor along the trajectory shown with the purple arrow. 10
2.4 The custom-designed controller board for interfacing with the sensors and actuators. The main components of the board are outlined with red rectangles. 11
2.5 Closed loop control system used in the force feedback experiments for rendering the stiffness of virtual objects. FSR readings of the inner and outer walls of the thimbles are summed and fed to the controller as positive and negative values, respectively. The force controller in the diagram outputs the voltage signal (V_m) for the first DC motor. The rotational velocity of the motor (ω_m) is converted to the translational motion of the sliders (x_{slider}) for grasping a virtual object. The displacements of the sliders are mapped to the displacements of the index finger and thumb (x_{finger}) in virtual worlds. The desired force to be displayed to the user is calculated based on the penetration depth of the virtual fingers into the virtual object. If there is no penetration, the desired force is set to zero by the switch S1, and the user freely moves the sliders till the virtual object is contacted by the fingers. 12
2.6 An earlier design iteration with the zoomed cross-sectional view from the datum plane A. The clearance between the grasper base and the top cover allows the free movement of the thimbles. However, when the user exerts a force on the thimbles, the slider rubs into the grasper base jamming the slider and restricting its motion. 14

2.7 Close-up view of the thumb thimble from the front of the device. The steel rods pass through the steel sleeves fixed inside the sliders. When the user exerts a force on the walls of the thimble, the torque generated about the brown axis causes frictional resistance and prevents the motor from being back-driven. 15

3.1 In the force stretch feedback experiments, two virtual objects are displayed side by side on the computer screen. The participants are asked to select the stiffer object by squeezing them. Participants had 15 seconds to answer each trial (they were given another 15 seconds if they could not answer within the first 15 seconds, which resulted in zero unanswered trials). Note that the device and the holding hand are covered with a cardboard box during the experiments. 17

3.2 Deformable behavior of the virtual objects displayed in our stiffness discrimination experiments was modeled by a simple linear elastic model, where they are assumed to be incompressible (The Poissons's ratio is equal to $\nu = 0.5$). When the user squeezes a virtual object using the index finger and thumb along the x direction, the object expands along the y and z directions to satisfy the incompressibility condition. 18

4.1 The results of the stiffness discrimination experiment when there is no conflict between visual and haptic cues. The dashed blue and red colored curves represent the participant's responses under H and VH conditions, respectively. The error bars show the standard deviations. A sigmoid function of the form $A/(1 + e^{-B(x-C)})$ was fitted to the average data with ΔK as the independent variable, and A, B, and C are the constant coefficients. R^2 value for both curves is 0.99. 22

4.2 The results of the stiffness discrimination experiment when there is variable conflict between visual and haptic cues. The results show that the discrimination performance of the participants was strongly affected by visual cues even for ΔK values much larger than those for which participants performed at almost 100% correct levels when there was no visual conflict. The error bars show the standard deviations. 23

4.3 A single-variable empirical model can successfully predict the results of the second set of experiments. The solid line represents the fitted curve. 24

4.4 Perceived stretch intensity as a function of tactor displacement and speed. 26

4.5 The skin stretch intensity perceived by the participants is modeled as a function of tactor displacement and velocity, utilizing the second order model given in (4.4). R^2 of the fit is 0.88. 28

A.1 Haptic device interface provides a graphical user interface to monitor and control the device over the serial port of a personal computer. . . 39

ABBREVIATIONS

VE	Virtual Environment
FSR	Force Sensitive Resistor
ASD	Apparent Stiffness Difference
JND	Just Noticeable Difference
UT	Upper Threshold
LT	Lower Threshold
ANOVA	Analysis of Variance
IMU	Inertial Measurement Unit

Chapter 1

INTRODUCTION

Displaying force feedback to a user in virtual environments through ungrounded actuated gloves and exoskeletons or grounded force-reflecting robotic arms has been extensively investigated (see the review of haptic devices for VR in Dangxiao et al. [Dangxiao et al., 2019] and Culbertson et al. [Culbertson et al., 2018]) These systems aim to provide high-fidelity haptic feedback, but limit users comfort and convenience by requiring them to attach bulky hardware to their arms as in ungrounded devices or by restricting the user to a small working space as in grounded devices. As an alternative, wearable and handheld devices have emerged for VR and gaming applications during the last decade.

Wearable haptic devices have been utilized to stimulate tactile (equivalently, cutaneous) receptors within the human skin or display object shape and material properties via net (resultant) force feedback. Chinello et al. [Chinello et al., 2017] developed a wearable fingertip device for rendering stiffness. In this system, three servo motors move an end-effector to simulate contacts of a finger with arbitrarily oriented surfaces. Bianchi et al. [Bianchi et al., 2016] developed a wearable device that can stretch a fabric sliding against the user's finger to render different levels of object stiffness. Gu et al. [Gu et al., 2016] designed a lightweight and wearable exoskeleton for displaying force feedback in VEs to multiple fingers of hand. Wolverine [Choi et al., 2016] is a low-cost wearable device which displays forces between the user's thumb and the three other fingers to simulate virtual objects being held in hand. Hinchet et al. [Hinchet et al., 2018] developed a wearable glove (DextrES) that utilizes electrostatic braking mechanisms to restrict users' finger motion, giving a sense of grasping virtual objects with the index finger and thumb. The readers may

refer to a taxonomy of wearable haptic devices for finger and hand in Pacchierotti et al. [Pacchierotti et al., 2017], and a more focused review of wearable gloves for VR in Perret and Poorten [Perret and Vander Poorten, 2018].

Handheld devices have been typically preferred over wearables by commercial companies marketing VR devices and controllers, such as Oculus Rift and HTC Vivo since they do not require attaching and detaching a device to the finger, hand, or body of a user. The haptic feedback provided by most of the commercial handheld haptic controllers is vibrotactile (cutaneous). The vibrotactile actuators are low-cost and small, hence easy to integrate into handheld devices, but limited in their ability to convey a sense of 3D shape and material properties such as softness. Ki-Uk Kyung and Jun-Young Lee developed the Ubi-Pen[Kyung and Lee, 2008], which utilized a single vibration motor to transmit vibration cues to the user and an embedded pin array to display virtual texture information to the user's fingertip. Arasan et al. [Arasan et al., 2015] embedded two vibration motors into a haptic stylus to generate a perceptual sense of bidirectional flow (known as phantom sensation) along the long axis of the stylus. They demonstrated the potential applications of this stylus in digital games played on a tablet.

In addition to vibrotactile, other actuation methods for displaying haptic feedback have been implemented with handheld devices. Guzererler et al. [Guzererler et al., 2016] designed a compact handheld haptic device that applies skin stretch to the palm which affords a larger area for deformation. They showed that not only the tactor displacement but also the velocity has a significant effect on the perceived intensity of shear force due to the viscoelastic nature of human skin. Whitmire et al. [Whitmire et al., 2018] developed a handheld controller which utilizes a rotating and interchangeable wheel at its tip to apply shear forces to the index finger of the user. Walker et al. [Walker et al., 2019] utilized two pantograph mechanisms attached to a handle to provide tangential displacements to the user's fingertips for motion guidance. Winfree et al. [Winfree et al., 2009] developed iTorqU, an ungrounded handheld device that utilizes a flywheel inside a two-axis actuated gimbal to generate directional torque feedback. Amemiya and Gomi [Amemiya and Gomi, 2012] used a handheld rotating flywheel to transmit directional torque feedback to a user.

Benko et al. [Benko et al., 2016] designed a handheld haptic controller to display the topography of virtual surfaces using a tiltable and extrudable platform and also their texture through a 4×4 matrix of actuated pins. Sinclair et al. devised CapstanCrunch[Sinclair et al., 2019], a handheld haptic device with a capstan-based brake whose resistance is controlled with a small DC motor to render compliant virtual objects without any active force control. Choi et al. [Choi et al., 2018] developed CLAW, a handheld haptic device that augments the typical VR controller functionality with force feedback to the index finger of the user, enabling grasping of virtual objects and exploring their surfaces.

Previous research has explored skin stretch on various body parts, including the forearm, foot, palm, and fingers. Prior investigations on tangential skin stretch have primarily concentrated on the fingertips. For instance, Paré et al. [Paré et al., 2002] conducted magnitude estimation experiments on seven participants to evaluate the perceived intensity of stretch under different loading rates and directions. They found that the perceived stretch intensity is linearly related to the applied force magnitude, regardless of the rate and direction. Gleeson et al. [Gleeson et al., 2010] developed a fingertip-mounted tactile device capable of stretching the fingerpad skin (i.e., applying shear force) to display directional cues to a user examined the effects of displacement, speed, and movement direction of the tactor on identifying the direction of stretch applied to the fingertip. Their study involved 11 participants who identified the directional cues accurately, with a 100% accuracy rate for 1mm displacement. The authors concluded that an increase in tactor speed significantly improves the perception of direction and that the direction of the cue also affects accuracy.

In summary, the industry and academia have a significant interest in wearable and handheld haptic devices for VR/AR/MR applications. Easy access to 3D printers nowadays enables to design and manufacture of wearable and handheld devices that are low-cost, lightweight, and replicable by others though their small form factor constrains the placement and selection of actuators and sensors utilized for haptic feedback. For the same reason, most of these devices provide only tactile cues composed of low forces. Moreover, even if the net force is the intended haptic

feedback, the range of forces that can be rendered by these devices is limited by the design due to their ungrounded nature.

We developed a cable-driven and handheld device for rendering the net forces involved in grasping and manipulating of 3D virtual objects (including soft ones) (Fig. 2.1). The handle of the device was designed to display tactile feedback to the palm via skin stretch for the haptic rendering of gravitational and inertial effects during the manipulation of 3D virtual objects. This allows for rendering additional sensory information and enhances the user's sense of presence and immersion in the virtual environment.

Compared to the earlier studies, we focused on the fine control needed to render the reaction forces arising during squeezing of soft virtual objects. We also aimed to design a handheld device that is simple and compact. For example, compared to the wearable and commercial exoskeleton devices such as CyberGrasp, Dexmo, HaptX, etc. (see Fig. 26 in Dangxiao et al. [Dangxiao et al., 2019]), our device can display force feedback to two fingers only, but this approach also simplifies the design and results in a device with a smaller form factor.

Using the proposed device, we demonstrate that the range of object stiffness perceived by the user in VEs can be expanded by manipulating the visual cues. It is already known that an individual's perceptual experience can be altered by manipulating the interactions between vision and touch. Earlier studies on human perception using real objects have shown that visual information can alter the haptic perception of object size, orientation, shape, and texture [Welch, 1986]. In the perception of size and shape [Warren and Rossano, 2013], when vision and touch provide conflicting information, humans rely on the visual cues more than the haptic ones, whereas in texture perception [Lederman and Abbott, 1981], they appear to use haptic cues as effectively as the visual ones. Moreover, the studies on human perception conducted in virtual environments have demonstrated that manipulation of force cues can also significantly alter our perception of object shape and surface. For example, the direction of the force vector reflected through a haptic device was altered in real-time to generate illusory bumps or troughs on an otherwise flat surface [Minsky, 1995], [Morgenbesser and Srinivasan, 1996]. Using this concept,

when force cues of a hole (bump) were combined with the geometric cues of a bump (hole), it has been shown that humans perceive a hole (bump) [Robles-De-La-Torre and Hayward, 2001], [Flanagan and Lederman, 2001]. It has also been shown that the visual perception of surface orientation can be altered by controlled haptic cues displayed through a haptic interface device [Ernst et al., 2000].

Most of the earlier multisensory experiments conducted in VEs have focused on the visual and haptic interactions for the perception of rigid objects, particularly their geometric and surface properties. Elastic objects, however, have the additional dimension of material properties such as their stiffness. While the deformable behavior of such objects can be rendered by visual and haptic displays in VEs (see the applications of this technology, for example, in medical simulation in rendering soft organ tissues with linear [Basdogan et al., 2001], nonlinear [Peterlik et al., 2010], and viscoelastic [Sedef et al., 2006] material properties), the force cues essential for the perception of their stiffness (or its reciprocal, the compliance) can only be obtained through touch [Srinivasan and LaMotte, 1995], though some more recent work suggests that people can infer compliance from indirect visual information alone [Drewing et al., 2009]. Although the visual and haptic perception of elastic materials [Srinivassan et al., 1996], [Wu et al., 1999], [Tiest and Kappers, 2009] and viscoelastic materials [Caldiran et al., 2019] has received some attention, their perception under the conflict of vision and touch has not been investigated in depth yet [Cividanes and Srinivasan, 2001].

In this thesis, we show how manipulated visual cues can be used to expand the range of stiffness perceived by the user in VEs. The physical range of stiffness of a virtual object that can be displayed to a user through a haptic device is typically limited by its resolution, bandwidth, and workspace. We show that the range perceived by the user can be effectively increased or decreased by altering the associated visual cues. We propose that a single variable, named Apparent Stiffness Difference, can predict the pattern of human stiffness perception under manipulated conflict, which can be used for rendering a range of soft objects in VEs larger than what is achievable by a haptic device due to its physical limits.

In addition, we conducted user studies to evaluate the palm stretch feedback

feature of the device. We showed that tactor displacement and speed play a significant role in the perceived intensity of skin stretch. The mapping between these two factors was found to be nonlinear. The results showed that the tactile sensitivity of the human palm to skin stretch applied by a tactor is uniform; stretch applied to the radial direction (towards the thumb) results in a similar intensity to that of the ulnar direction (away from the thumb).

Chapter 2

DESIGN OF THE HANDHELD HAPTIC DEVICE

Our handheld haptic device consists of mainly two parts: grasper and handle (Fig. 2.1). The handle of the device is made of 2 half-cylinders, each containing a DC motor (DCX16S EB KL 6V, Maxon Inc.) for the actuation of cable-driven force feedback and stretch mechanisms. The device weighs 225 grams in total.

2.1 Grasper with Force Feedback

The grasper can simulate holding a 3D object with the index finger and thumb to display its stiffness to the user in VEs. An electric motor and a cable-driven mechanism made of 4 pulleys (one for tensioning) and a coated steel wire (Fig. 2.1) were used to control the sliding movements of the thimbles, where the index finger and thumb are inserted, to display force feedback to the user during the grasping of a virtual object. A pressure sensor (FSR 402, Interlink Electronics Inc.) was placed inside the side walls of each thimble (see the zoomed view in Fig. 2.1) to measure the grasping forces applied by the fingers when holding and releasing the virtual object. The thimbles can rotate freely around the axis normal to the sliding direction to fit over the fingers of the user easily and for comfortable sliding. Thimbles have a linear motion range of 47.5 mm. The pressure sensors were calibrated by using known weights priori.

2.1.1 Force Tracking

When there is no virtual object to grasp, the user moves their fingers freely without any resistance. However, as shown in Fig. 2.2, the user needs to exert at least 0.3 Newtons of force before the motor actuates and compensates for the force error (desired - actual). That is due to the break force (turn-on force) of the FSR sensor.

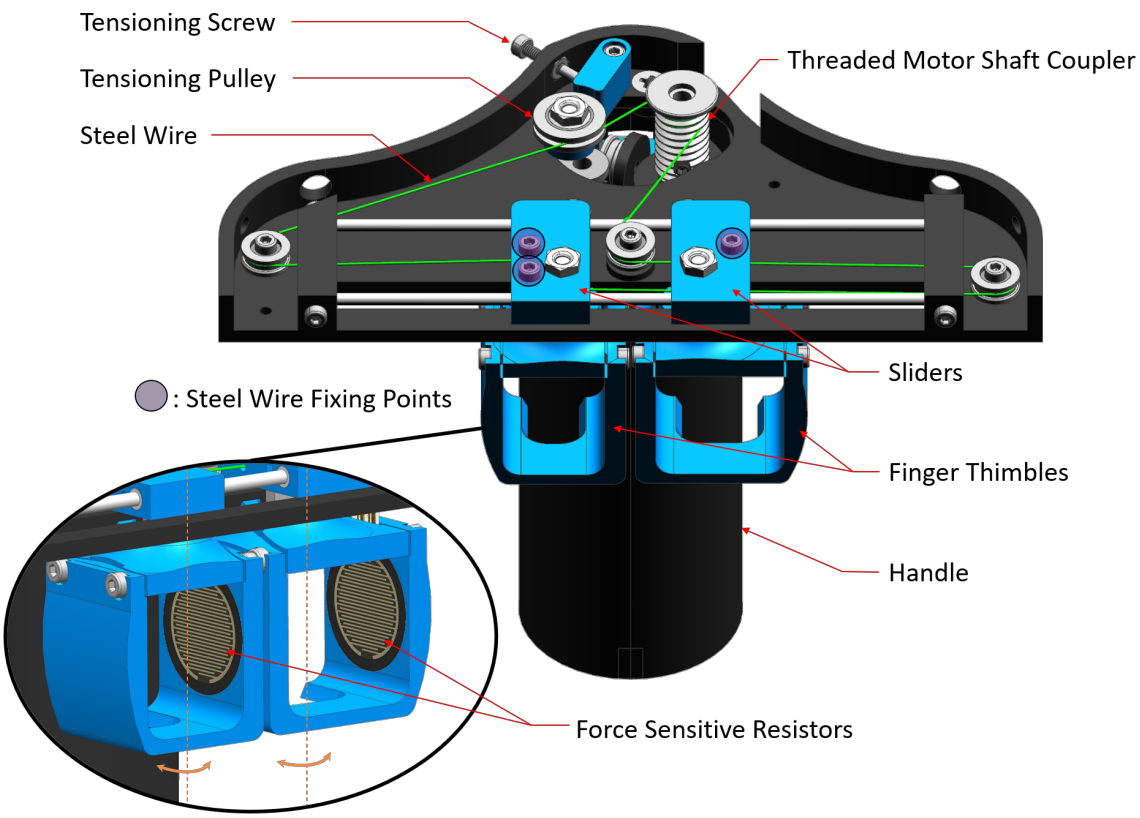

Figure 2.1: Internal structure of our handheld haptic device and the close-up view of the thimbles. The electric motor inside the handle (not shown) rotates and translates the thimbles in accordance with the forces applied by the index finger and thumb, which are measured by the pressure sensors attached to the inner walls of the thimbles. This allows a resistance-free movement of the fingers when there is no contact with the virtual object and renders its stiffness when there is. For easy fit to fingers and comfortable use of the device, the thimbles can passively rotate around the vertical axis shown in the close-up view.

Break force is the minimum force required to cause the onset of the FSR response for a given sensor size [InterlinkElectronics, 2018]. Hence, the break force of the FSR sensor determines the minimum stiffness value that can be rendered with our

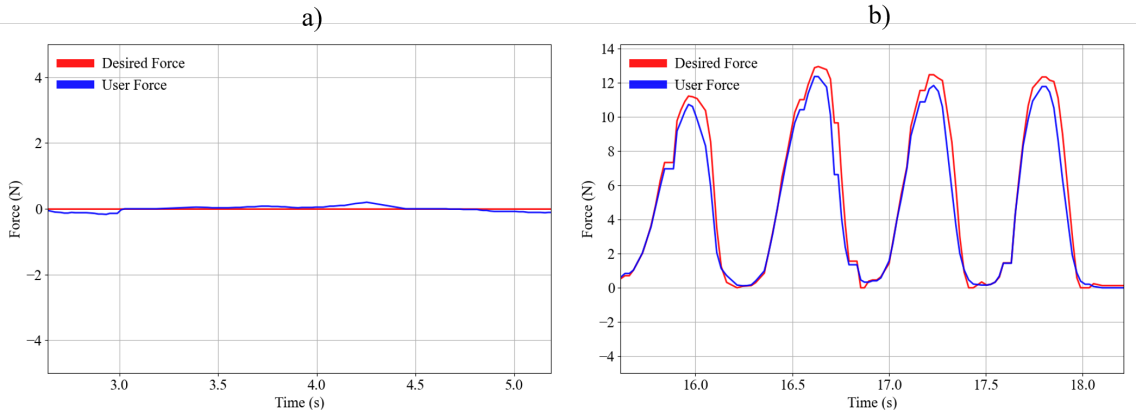

Figure 2.2: The motor actuates and moves the sliders to match the applied user force (measured by the FSR sensors) with the desired force. Note that the positive and negative values of user force are the sum of the forces read from the FSR sensors on the inner and outer walls of the thimbles, respectively. a) Desired force is equal to zero when there is no contact with the virtual object. b) The user and desired forces are shown as the user repetitively squeezes the virtual object. The desired force changes as the user moves their fingers while holding the object. The user force lags behind the desired force, and the force controller aims to compensate for the lag by adjusting the motor speed.

haptic device. When the user grasps the object with two fingers, the desired force is determined based on the depth of penetration of the fingers into the virtual object. The motor then actuates and moves the sliders to compansate for the difference between the measured force and the desired force.

2.2 Handle with Stretch Feedback

An elliptical rubber pin attached to a tactor moving along the device handle stretches the palm for tactile feedback. The device handle has a diameter of 37 mm. The tactor located at the back of the device, as shown in Fig. 2.3, moves parallel to the handle's longitudinal axis. When the user grasps the device by the handle, the moving tactor stretches the palm skin of the user along the radial and ulnar

h

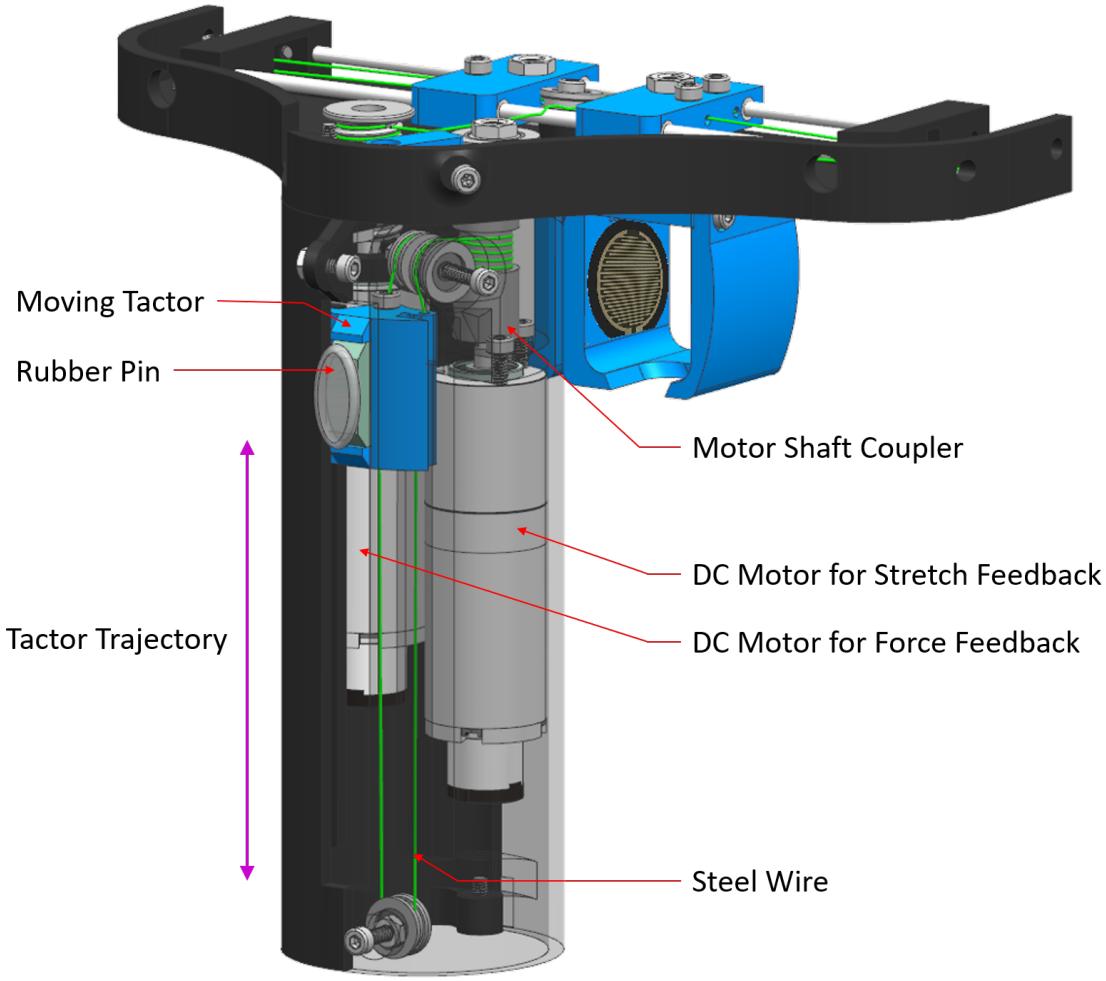

Figure 2.3: Back view of the haptic device with one of the half cylinders of the handle displayed transparently to show the device's internals. Cable-driven mechanism translates the rotation of the motor shaft into the translational motion of the tactor along the trajectory shown with the purple arrow.

directions. A separate cable-driven mechanism, made of 3 pulleys and a coated steel wire, is actuated by the second DC motor inside the handle to translate the moving tactor. The tactor has a linear motion range of 40 mm.

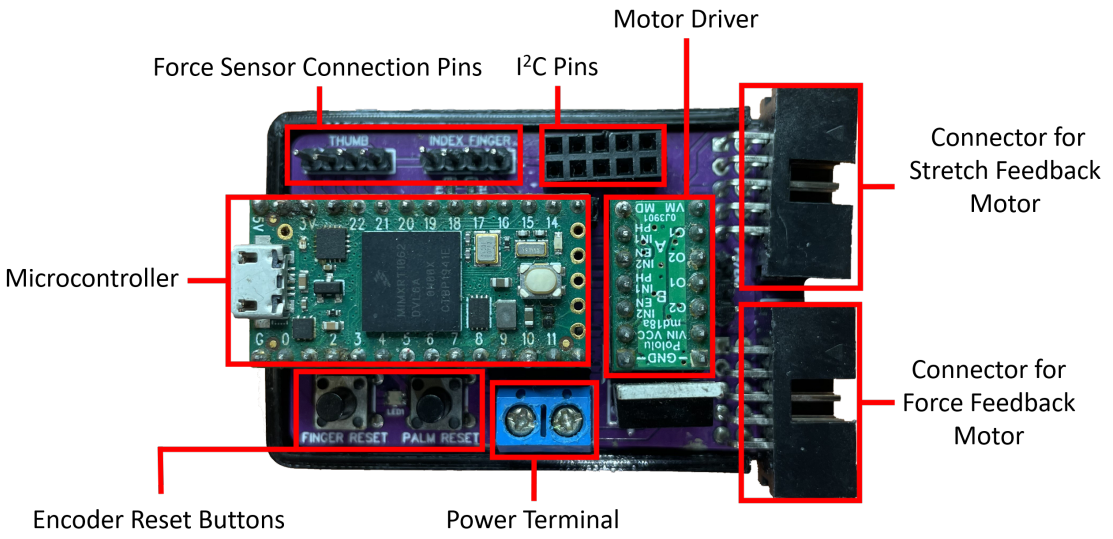

Figure 2.4: The custom-designed controller board for interfacing with the sensors and actuators. The main components of the board are outlined with red rectangles.

2.3 Controller Board

We have designed a custom controller board (Fig. 2.4) to access and control the components of the device. The board communicates with a personal computer through a serial port. A microcontroller (Teensy 4.0 Development Board, PJRC Inc.) on the board is utilized to interface with the sensors and actuators of the haptic device. For displaying force feedback through the grasper, the microcontroller reads the changing resistance values of the FSR sensors. It calculates the forces applied by the index finger and thumb based on a priori-determined calibration curve. Then, A PID controller deployed on the microcontroller minimizes the error between the measured and desired forces by adjusting the rotational speed of the first motor responsible for displaying force feedback to the fingers. The closed-loop control architecture for rendering the stiffness of virtual objects is shown in Fig 2.5.

For displaying stretch feedback through the tactor at the handle, another PID controller is implemented to regulate the rotational speed of the second motor in order to adjust the linear velocity and position of the tactor stretching the palm. Since the motors' encoders are not absolute but incremental, push buttons installed on the

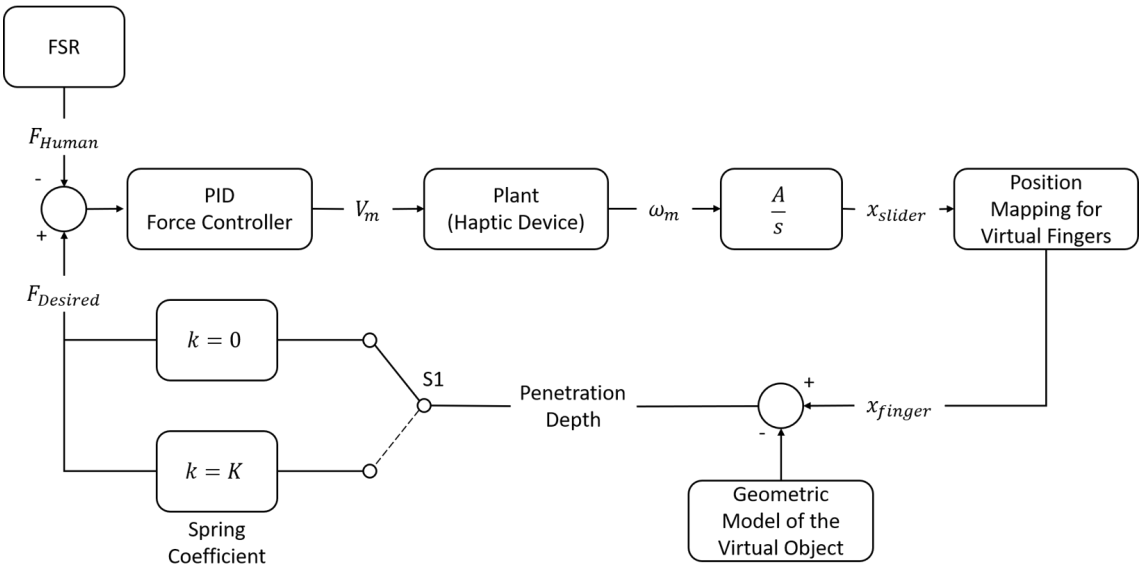

Figure 2.5: Closed loop control system used in the force feedback experiments for rendering the stiffness of virtual objects. FSR readings of the inner and outer walls of the thimbles are summed and fed to the controller as positive and negative values, respectively. The force controller in the diagram outputs the voltage signal (V_m) for the first DC motor. The rotational velocity of the motor (ω_m) is converted to the translational motion of the sliders (x_{slider}) for grasping a virtual object. The displacements of the sliders are mapped to the displacements of the index finger and thumb (x_{finger}) in virtual worlds. The desired force to be displayed to the user is calculated based on the penetration depth of the virtual fingers into the virtual object. If there is no penetration, the desired force is set to zero by the switch S1, and the user freely moves the sliders till the virtual object is contacted by the fingers.

board are utilized to reset the encoder positions. An integrated circuit (DRV8835, Texas Instruments Inc.) drives both motors. A custom desktop app (Fig. A.1) sends commands to the controller board and displays the device status on the PC.

2.4 Earlier Designs

The design process involved many iterations before the actual device was realized. In one of the earlier iterations (Fig 2.6), the sliders and thimbles were a single piece, and the sliders used to rely on the clearance between the top cover and the grasper base to slide. It should also be noted that this design lacks outer walls on the thimbles meaning the releasing forces of the fingers are not captured. This design was easier to manufacture and assemble due to having fewer parts. However, undesired friction between the parts adversely affected the rendering of virtual objects. To overcome this problem, we utilized two stainless steel rods that pass through the stainless steel sleeves, which were securely fitted inside the sliders (Fig. 2.7). Unfortunately, this design prevents the force feedback motor from being back-driven because when the user exerts a force on the thimble walls, the friction force between the sleeve and rod dramatically increases due to the undesired torque generated about the radial axis of the rod. In the most recent design (Fig. 2.7), the steel wire pulls the sliders from the center and does not generate any undesired torques. The new design also incorporates a tensioning pulley to keep the steel wire tight, which is required for minimal backlash.

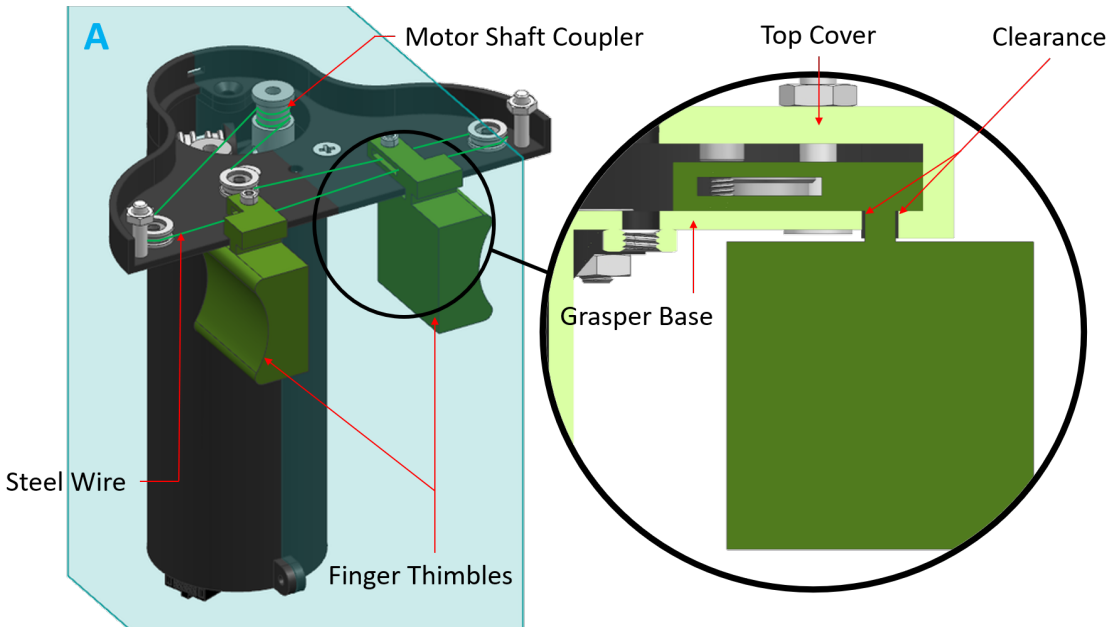

Figure 2.6: An earlier design iteration with the zoomed cross-sectional view from the datum plane A. The clearance between the grasper base and the top cover allows the free movement of the thimbles. However, when the user exerts a force on the thimbles, the slider rubs into the grasper base jamming the slider and restricting its motion.

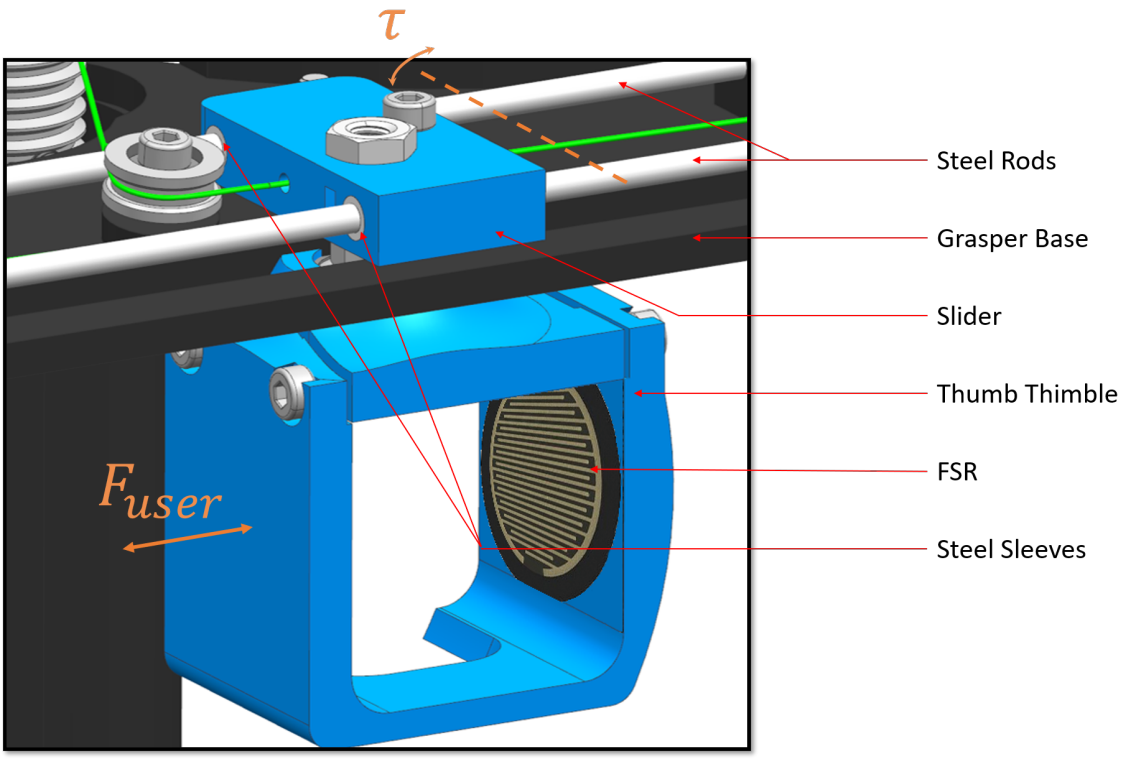

Figure 2.7: Close-up view of the thumb thimble from the front of the device. The steel rods pass through the steel sleeves fixed inside the sliders. When the user exerts a force on the walls of the thimble, the torque generated about the brown axis causes frictional resistance and prevents the motor from being back-driven.

Chapter 3

EXPERIMENTS

3.1 Force Feedback Experiments

We conducted two sets of human psychophysical experiments to investigate the effect of manipulated visual information on the haptic perception of object stiffness in VEs [Srinivassan et al., 1996], [Wu et al., 1999], [Cividanes and Srinivasan, 2001]. During the experiments, a pair of virtual objects in the shape of a rectangular box was displayed side by side to the participants visually on a computer monitor and haptically via the handheld haptic device introduced in this study (Fig. 3.1). It is assumed that the virtual objects are purely elastic and incompressible, having a Poisson's ratio of 0.5 in each direction. In the first set of experiments, participants were asked to discriminate the stiffness of the objects using haptic cues with and without a visual display of the haptic deformations. In the second set of experiments, the same participants were asked to repeat the same task, but the relationship between the visually presented deformation and the haptic deformation of each object was varied among the experimental trials to investigate the effect of manipulated visual cues on the haptic perception of object stiffness.

In the first set of experiments, the stiffness of one of the objects (reference) was kept constant ($K_0 = 2\ N/mm$), while the stiffness of the other (variable) was set to $K_0 + \Delta K$, with ΔK varying from –30% to 30% of K_0. A total of 6 naive participants (2 females, 4 males; the average age is 26 $\pm$ 3 years, with no known physical impairments) participated in the experiments, and they were asked to discriminate the stiffness of the objects by squeezing the objects with their index finger and thumb and judging which one was stiffer. The participants were prevented from seeing their own hand. The experiments were conducted under two conditions: (1) only haptic cues were provided to the participants (H) and (2) both visual and

Figure 3.1: In the force stretch feedback experiments, two virtual objects are displayed side by side on the computer screen. The participants are asked to select the stiffer object by squeezing them. Participants had 15 seconds to answer each trial (they were given another 15 seconds if they could not answer within the first 15 seconds, which resulted in zero unanswered trials). Note that the device and the holding hand are covered with a cardboard box during the experiments.

haptic cues were provided together to the participants (VH). The haptic stimulus was generated by the handheld haptic device, and the visual cues were displayed on a computer monitor. There were in total 7 stiffness pairs ($\Delta K/K_0$ = -30%, -20%, -10%, 0, 10%, 20%, and 30%) $\times$ 2 conditions (haptics only or both vision and haptics

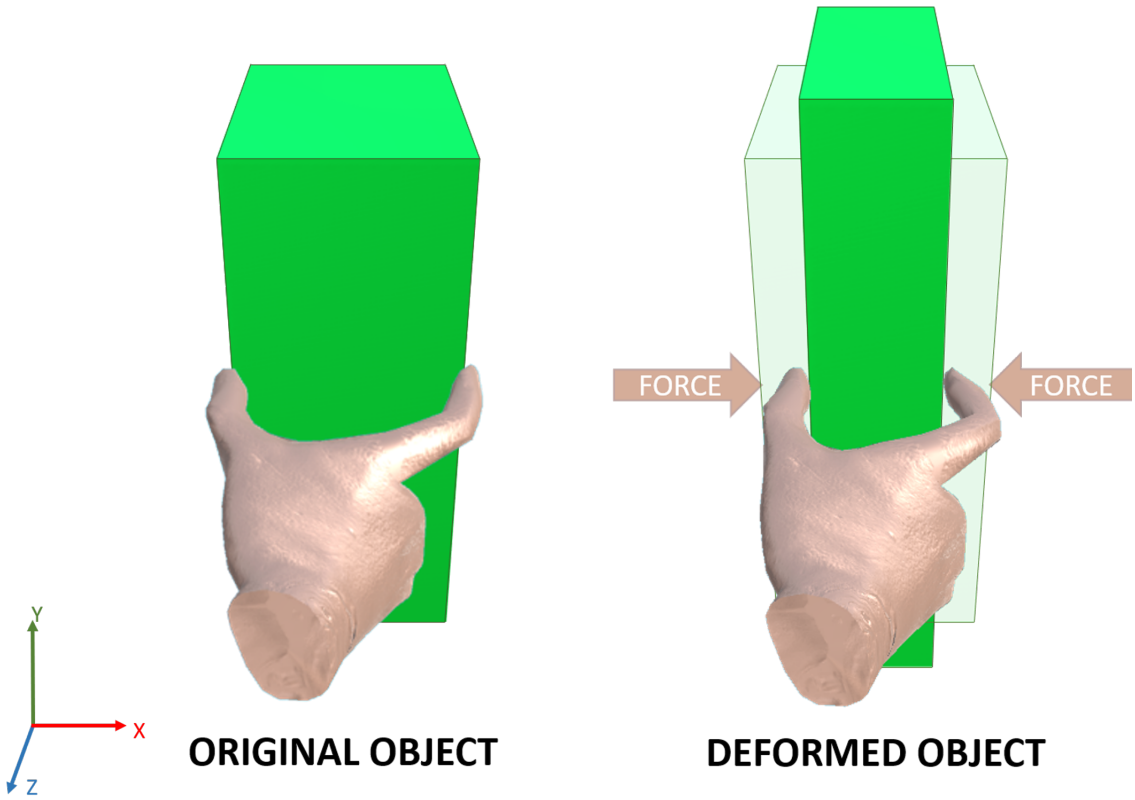

Figure 3.2: Deformable behavior of the virtual objects displayed in our stiffness discrimination experiments was modeled by a simple linear elastic model, where they are assumed to be incompressible (The Poissons's ratio is equal to $\nu = 0.5$). When the user squeezes a virtual object using the index finger and thumb along the x direction, the object expands along the y and z directions to satisfy the incompressibility condition.

together) = 14 cases, with 10 trials for each case. The order of the trials in each case (visual cues present or absent) was randomized, with the same order displayed to each participant.

A total of 11 participants (7 females, 4 males; the average age is 25 $\pm$ 3 years, with no known physical impairments) participated in the second set of experiments. This time, the visual display of the deformation of each object was manipulated across the experimental trials. In each trial, the stiffness of one object was always equal to a reference stiffness, $K_0 = 2\ N/mm$. The stiffness of the other was ($K_0 +$

ΔK), ΔK being $0.25K_0$, $0.5K_0$, $0.75K_0$, or K_0. Trials were randomized so that the stiffness of both objects had an equal probability of having the reference stiffness. The participant could not have prior knowledge of which object was stiffer. The following set of equations determined the relationship between the haptic and visual deformation of each object:

$$\begin{aligned} X_{h,reference} &= \frac{F}{K_0} \\ X_{v,reference} &= \frac{F}{(1-\lambda)K_0 + \lambda(K_0 + \Delta K)} \\ X_{h,variable} &= \frac{F}{K_0 + \Delta K} \\ X_{v,variable} &= \frac{F}{(1-\lambda)(K_0 + \Delta K) + \lambda K_0} \end{aligned} \tag{3.1}$$

where $X_{h,reference}$ and $X_{v,reference}$ are the haptic and visual displacements of the reference object, respectively. Similarly, the relations for $X_{h,variable}$ and $X_{v,variable}$ represent the haptic and visual displacements of the variable object, respectively. λ is a parameter that manipulates only the visual deformation, and its value was equal to 0, 0.25, 0.50, 0.75, or 1 in the experiments. In this way, λ ranged from zero conflict ($\lambda = 0$), that is, the visual deformation of each object corresponded to its haptic deformation, to a case of a complete conflict ($\lambda = 1$), where the visual displacement of the object with the stiffness of K_0 was equal to the haptic displacement of the other object with the stiffness of $K_0 + \Delta K$ for the same force F and vice versa. As in the first experiment, participants were asked to discriminate the softness of the objects by judging which one was stiffer. Participants were just told to look at the screen. No emphasis was made on whether they should focus on the visuals or the haptic sensation. There were in total 4 stiffness pairs ($\Delta K/K_0$ = 25%, 50%, 75%, and 100%) $\times$ 5 different settings of λ (0, 0.25, 0.5, 0.75, and 1) = 20 cases with 10 trials for each case per participant. The stimuli order was randomized among ΔK and λ, displaying the same order for each participant.

3.2 Stretch Feedback Experiments

We conducted a magnitude estimation experiment as in [Guzererler et al., 2016] to investigate the perceived magnitude of stretch applied to the palm based on tactor displacement, speed, and direction. The experiment involved five participants (2 females and 3 males), who were all right-handed and had no known sensorimotor problems, with an average age of 26 ± 2 years. The stretch stimulus was a combination of three different tactor displacements (4, 8, and 16 mm), three different tactor speeds (5, 32.5, 60 mm/s), two different movement directions of the tactor with respect to the palm (radial: towards the thumb, and ulnar: away from the thumb). Displacement and speed values were selected by considering the physical capabilities of the device. In total, 108 stimuli (3 displacements $\times$ 3 speeds $\times$ 2 directions $\times$ 6 repetitions) were applied to the right palm of each participant in a single session. During each stimulus, the tactor moved from the center position and followed a trapezoidal velocity profile where the ramp period of the trapezoidal curve was significantly shorter than the constant speed period. After the desired position was reached and the participant entered their response (i.e. perceived magnitude and direction), the tactor moved back to the center position. Before the experiment, participants were informed about the nature of the experiment and instructed to grasp the device with a certain amount of force in a comfortable manner. During the experiment, participants were asked to wear headphones playing white noise to block the motor's noise. A soft pad was placed under the elbow of the participants to reduce fatigue. Participants were presented with a training session displaying all possible combinations of stimuli before the actual experiment. During the actual experiment, participants reported the estimated direction of the tactor movement (up/down) and the perceived magnitude of the stimuli as a scalar number on a scale of 0 to 9999. The stimuli were displayed randomly to each participant while maintaining the same order among the participants. The experiment was completed within approximately 30 minutes.

Chapter 4

RESULTS

4.1 Results of Force Feedback Experiments

The results of the first set of experiments (Fig. 4.1), plotted as the percentage of trials in which the variable object was perceived to be stiffer than the reference object versus stiffness increment ΔK (expressed as a percent of K) show that when $|\Delta K|$ was greater than 10%, the participants could discriminate the stiffnesses of two buttons at almost 100% correct through haptics with or without the supporting visual information. The Just Noticeable Differences (JND) under the H and VH conditions were estimated from the psychometric curve as 10.41% and 7.24%, respectively. These values are in line with the ones reported in the literature [Drewing et al., 2009], [Caldiran et al., 2019], [Tan et al., 1992], [Tan et al., 1994], [Lécuyer et al., 2000]. Two-way ANOVA (analysis of variance) showed a significant effect of ΔK ($F_{6,70} = 56.7$, $p < 0.0001$) and vision ($F_{1,70} = 5.9$, $p = 0.018$), and no interaction between the two ($F_{6,70} = 1.7$, $p = 0.13$).

The results of the second set of experiments (Fig. 4.2) showed that the percentage of correct responses decreased significantly as the conflict between visual and haptic cues was increased. Two-way ANOVA showed a significant effect of λ ($F_{4,200} = 211.0$, $p < 0.0001$), no effect of ΔK ($F_{3,200} = 0.6$, $p = 0.61$), and no interaction between the two ($F_{12,200} = 1.6$, $p = 0.10$). For example, at full conflict ($\lambda = 1$) when the visual displacement of the object with the stiffness of $K_0 + \Delta K$ at a given force was equal to the haptic displacement of the object with the stiffness of K_0 and vice versa, the participants were wrong more than 70% of times in their judgments. This total reversal of results compared to their performance when there was no conflict ($\lambda = 0$) is unexpected, considering that the ΔK values used in these experiments were such that the participants would be able to discriminate the stiffnesses correctly at

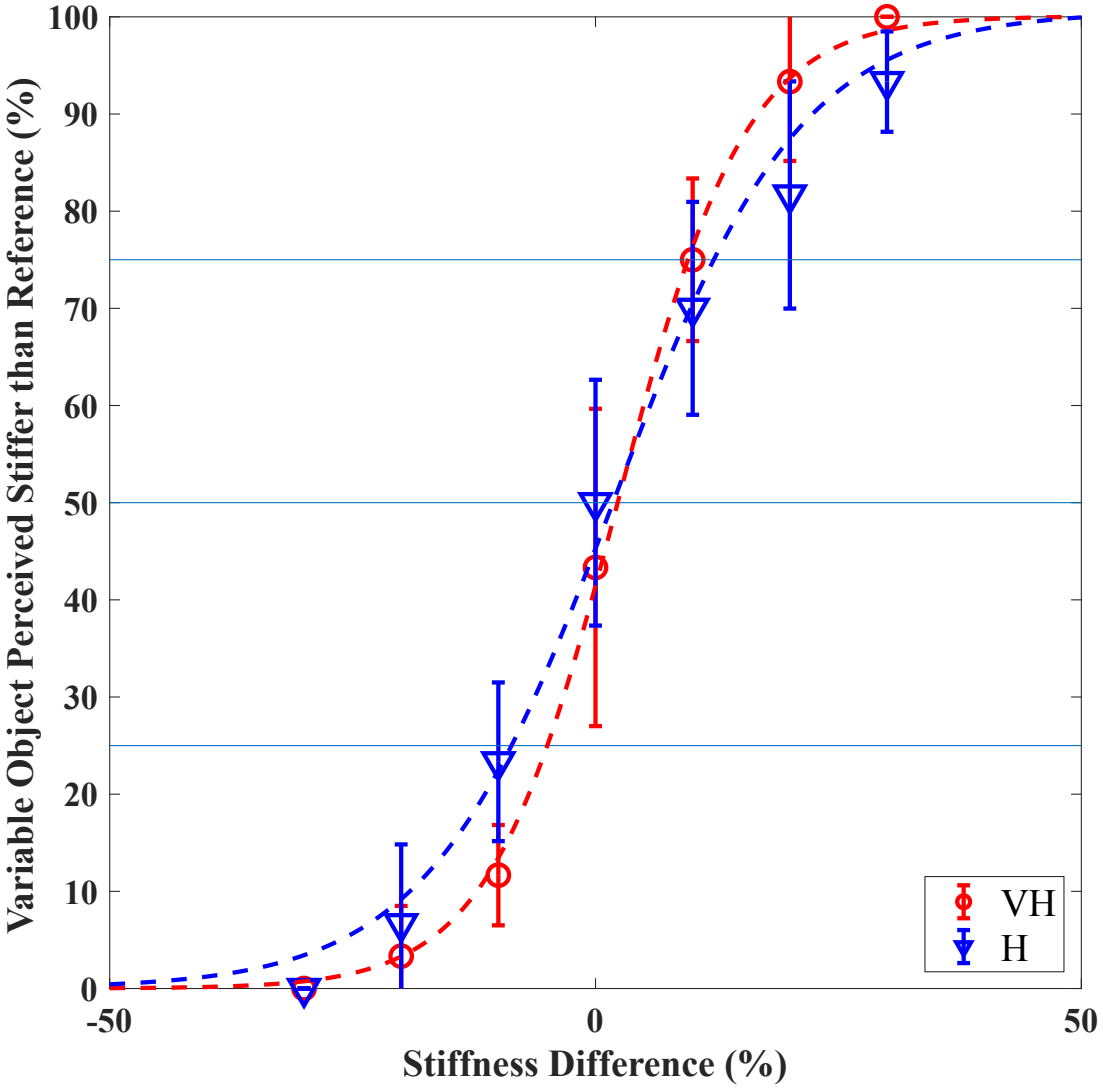

Figure 4.1: The results of the stiffness discrimination experiment when there is no conflict between visual and haptic cues. The dashed blue and red colored curves represent the participant's responses under H and VH conditions, respectively. The error bars show the standard deviations. A sigmoid function of the form $A/(1+e^{-B(x-C)})$ was fitted to the average data with ΔK as the independent variable, and A, B, and C are the constant coefficients. R^2 value for both curves is 0.99.

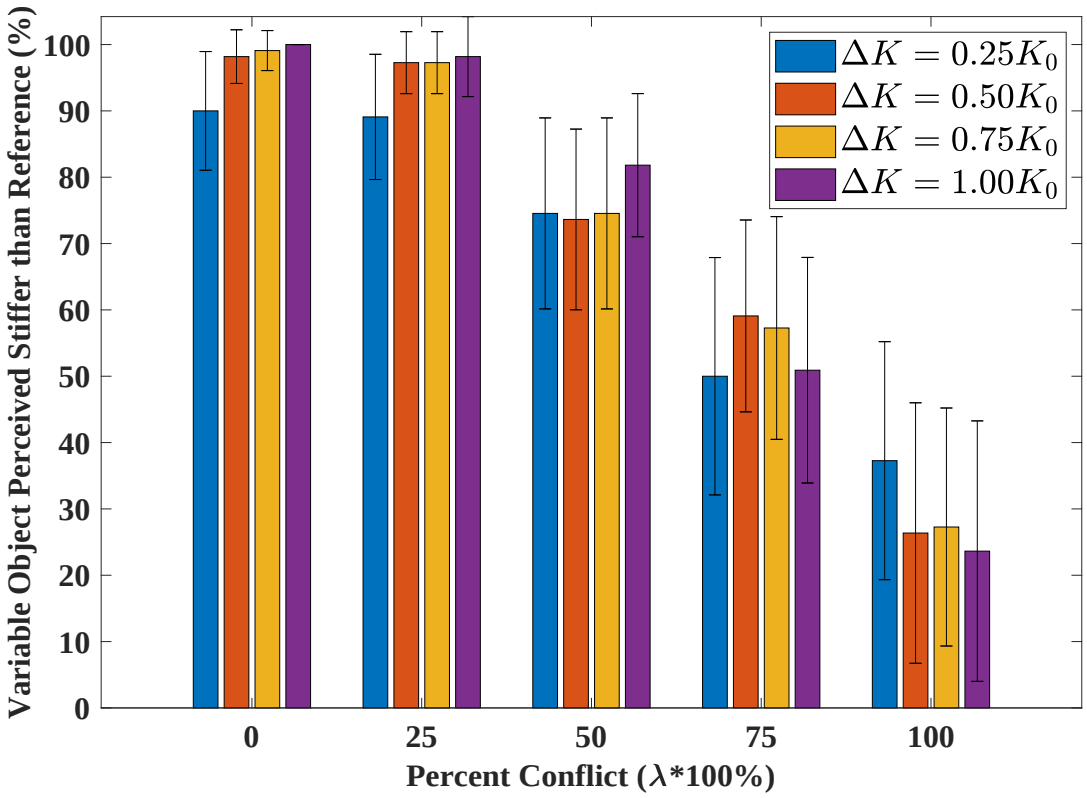

Figure 4.2: The results of the stiffness discrimination experiment when there is variable conflict between visual and haptic cues. The results show that the discrimination performance of the participants was strongly affected by visual cues even for ΔK values much larger than those for which participants performed at almost 100% correct levels when there was no visual conflict. The error bars show the standard deviations.

100% even with the haptic information alone, as indicated by the results of the first experiment.

The strong dependence of participants' stiffness discrimination on the visual information suggests the following analysis. By definition, the computation of the stiffness of an object requires the determination of the ratio of the force applied to the resulting deformation. In the discrimination experiments involving visual and haptic cues, the force information has to necessarily come from the haptic channel, whereas the deformation information has two alternative paths: the displacement

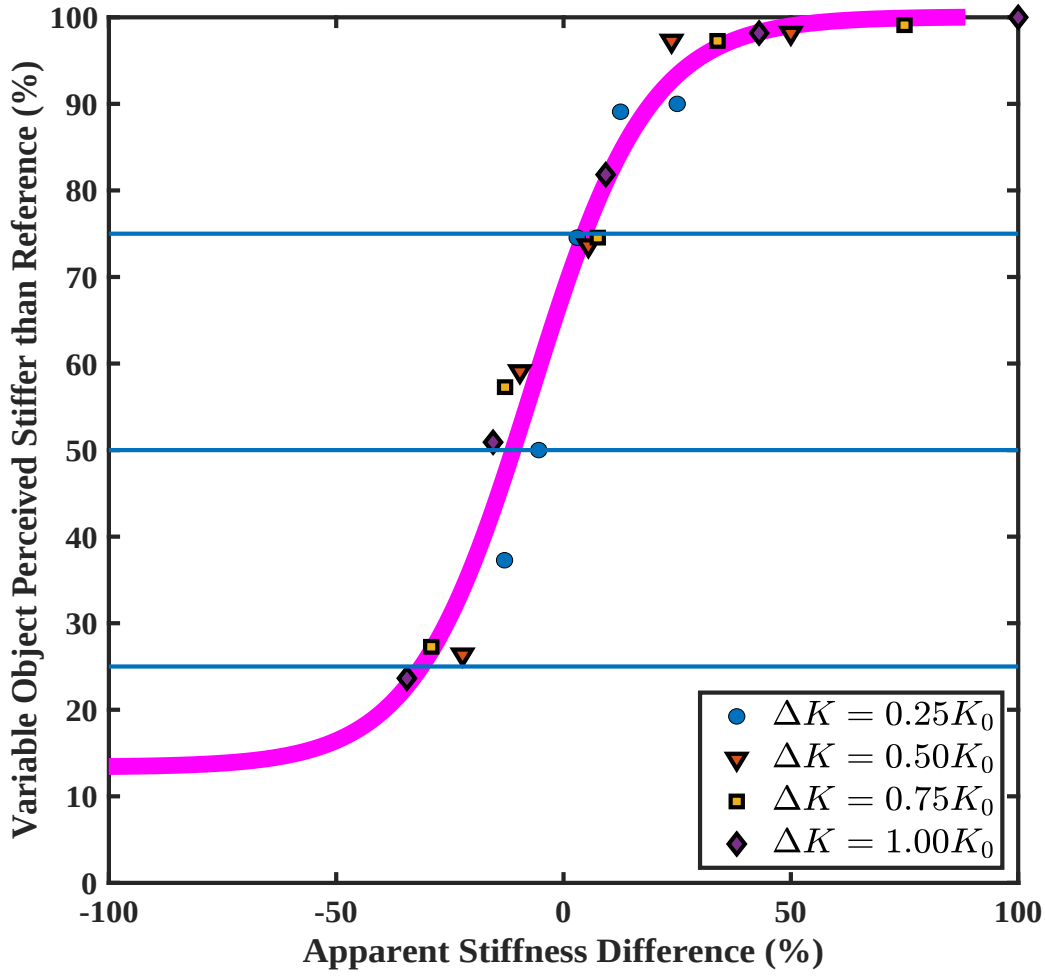

Figure 4.3: A single-variable empirical model can successfully predict the results of the second set of experiments. The solid line represents the fitted curve.

of the real fingers sensed kinesthetically and the displacement of the virtual fingers sensed visually. The results of the second experiment then suggest the following hypothesis: when there is a conflict in the displacement information from the two paths, the participant relies on visual displacement and associates it with the applied force sensed haptically while paying less attention to the haptic displacement information sensed kinesthetically. In this regard, we could reformulate the discrimination problem as follows. The stiffness of the reference object perceived by the participant ($K_{reference}$) will be the applied force (F) divided by the visual displacement of the reference object ($X_{v,reference}$) and the stiffness of the variable object

perceived by the participant ($K_{variable}$) will be the applied force, F, divided by the visual displacement of the variable object ($X_{v,variable}$). However, as seen in Fig. 4.2, the uncertainty in the response of participants increased as the conflict between vision and touch was increased. To address this issue, we update λ by taking the standard error of the means of the participants' responses into account. Hence, λ' is defined as:

$$\lambda' = \frac{(100 - \bar{\sigma})}{100} \times \lambda \tag{4.1}$$

where $\bar{\sigma}$ is the average of the standard error of means of the different ΔK values for a given λ. Then, it follows from the equations given in (3.1), $K_{reference}$ and $K_{variable}$ can be calculated as:

$$\begin{aligned} K_{reference} &= (1 - \lambda')K_0 + \lambda'(K_0 + \Delta K) \\ K_{variable} &= (1 - \lambda')(K_0 + \Delta K) + \lambda' K_0 \end{aligned} \tag{4.2}$$

The stiffness discrimination judgments made by the participants would then be based on Apparent Stiffness Difference (ASD), which is defined as:

$$ASD = 100 \times (\frac{K_{variable} - K_{reference}}{K_{reference}}) \tag{4.3}$$

To test this hypothesis, the experimental data was re-plotted against ASD (Fig. 4.3). To obtain a predictive model, a sigmoid curve of the form $A/(1 + e^{-B(x-C)}) + D$ was fitted to the average data with ASD as the independent variable, and A, B, C, and D are the constant coefficients ($R^2 = 0.96$). The JND was estimated from the psychometric curve as 17.9%. The asymmetry in the psychometric curve can be observed from the difference between the values of upper and lower thresholds (UT = 4.6%, LT = −31.2%), which needs further investigation.

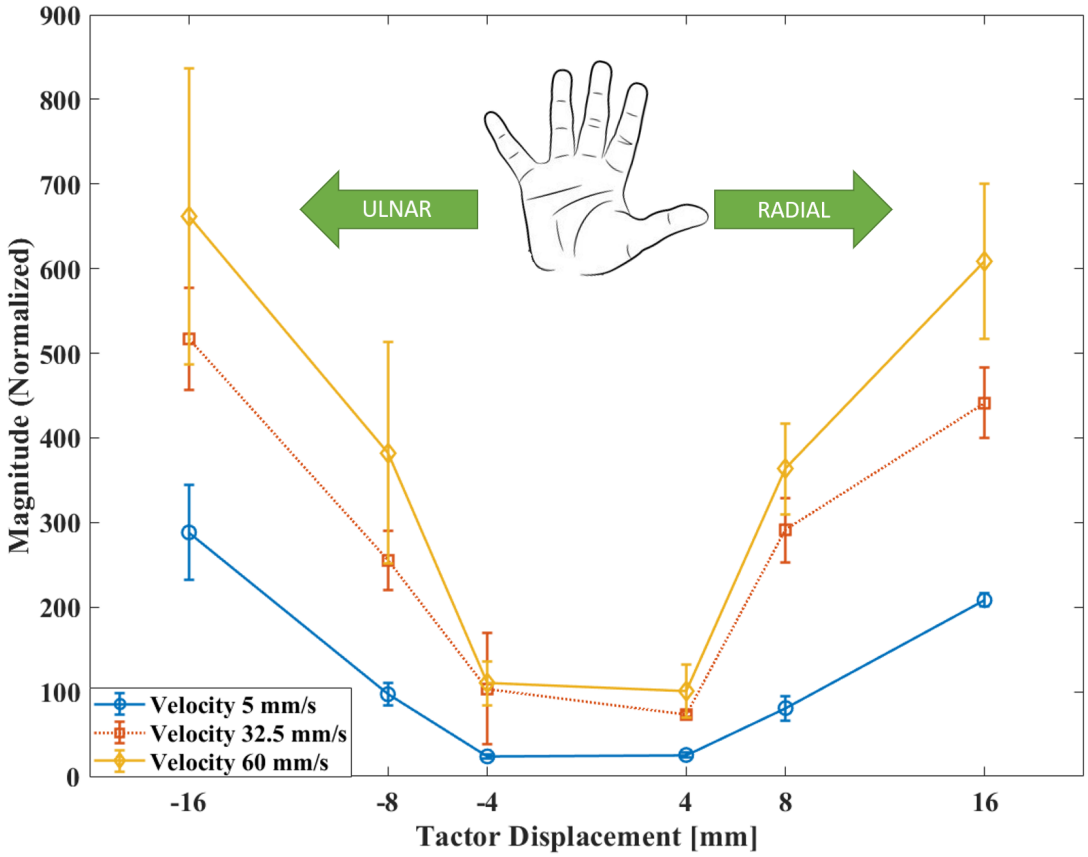

Figure 4.4: Perceived stretch intensity as a function of tactor displacement and speed.

4.2 Results of Stretch Feedback Experiments

The subjects could accurately discern the direction of the tactor's motion, achieving a high accuracy rate of 97.96 ± 3.26%. The lowest level of accuracy achieved by the participants is 86.67 ± 13.94%, which occurred when the tactor was displaced by 4 mm with a speed of 5 mm/s in the ulnar direction.

To eliminate the inter variability in the participants' magnitude response (since the participants were free to choose any positive number between 0 and 9999 for the perceived intensity), we normalized the data as suggested by Murray et al. [Murray et al., 2003]. Initially, we divided their individual response recorded for an experimental condition by their own geometric mean and then multiplied it by the overall geometric mean of all participants for that condition. Since the participants

were allowed to give their magnitude response on a large scale (0-9999), the geometric mean is preferred over arithmetic mean to account for the exponential nature of the given answers.

We performed 3-way repeated measures ANOVA on the normalized perceived magnitudes. The results of our study demonstrated that both speed ($F_{2,87} = 162.84$, $p < 0.001$) and displacement ($F_{2,87} = 60.17$, $p < 0.01$) significantly affected the perceived intensity of skin stretch, as expected. However, the stretch direction did not significantly affect the perceived intensity ($F_{1,88} = 2.79$, $p = 0.17$). We also discovered that there was an interaction effect between displacement and speed ($F_{4,40} = 124.02$, $p < 0.05$) as well as direction ($F2, 27 = 12.28$, $p < 0.05$).

The results of the ANOVA analysis showed that the stretch intensity is influenced by both speed and displacement, with a significant interaction effect between the two. Therefore, we developed a second-order model for estimating the perceived stretch intensity of the participants as a function of displacement, velocity, and the interaction between the two (see Eq. (4.4)). Fig. 4.5 shows the curve-fit of the model to the averaged intensity data of all participants. Table 4.1 summarizes the coefficients of the model.

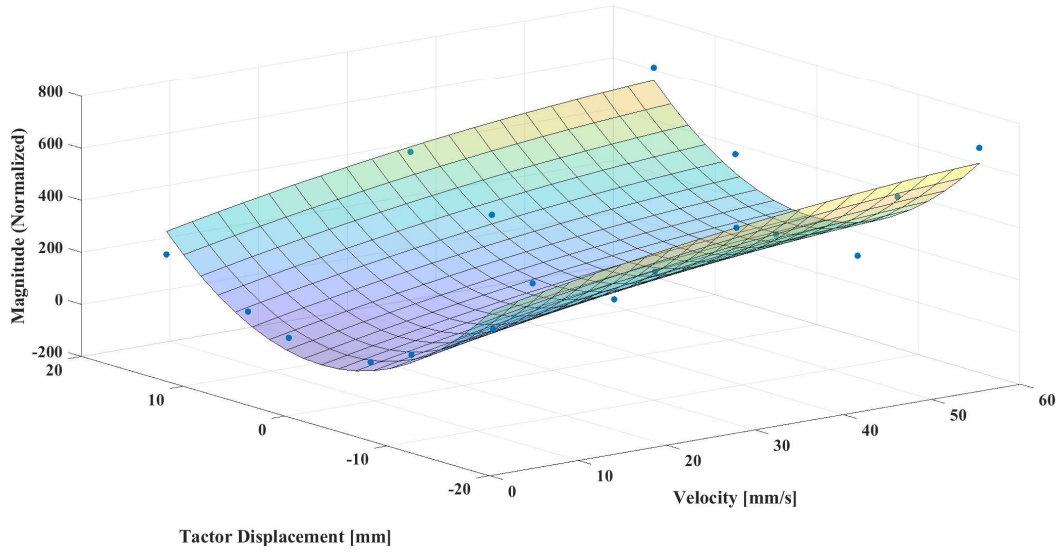

Figure 4.5: The skin stretch intensity perceived by the participants is modeled as a function of tactor displacement and velocity, utilizing the second order model given in (4.4). R^2 of the fit is 0.88.

	A	B	C	D	E	F
Φ	-0.05	1.45	7.52	-2.05	0.01	-77.91

Table 4.1: Coefficients of the proposed model.

$$\Phi(v, x) = Av^2 + Bx^2 + Cv + Dx + Evx + F \tag{4.4}$$

In the equation, perceived intensity of palm stretch (ϕ) is given as a function of tactor velocity (v) and displacement(x).

Chapter 5

DISCUSSION

The results of the force feedback experiment suggest that visual position information has a clear dominance over the haptic hand position information in the discrimination of object stiffness when there is a conflict between visual and haptic cues. The participants essentially paid less attention to kinesthetic hand position information regarding object deformation, and based their judgment on the relationship between the visual position information and the indentation force sensed haptically. This result has the practical application that while the physical range of stiffnesses of virtual objects that can be displayed to a user is typically limited by the resolution, bandwidth, and the workspace of the haptic device, the range perceived by the user can be effectively increased or decreased by altering the associated visual cues. There is, however, an asymmetry in the human perception of such manipulated visual information (as seen in Fig. 4.3), which warrants further investigation.

The results of stretch feedback experiments show that the tactor displacement and the velocity have a significant effect on the perceived intensity of shear force due to the viscoelastic nature of human skin, as suggested by [Guzererler et al., 2016].

In contrast to what was reported in [Guzererler et al., 2016], the direction of the stretch in our experiments did not have a significant effect on the perceived intensity of skin stretch intensity at the palm of the participants. The differences in the form factor of the devices, tactor geometries and the material properties of the tactor pins could be the underlying causes for such an outcome. For example, in our design, when the users grasp the device by the handle, unlike the design by [Guzererler et al., 2016], their thumb and index fingers do not wrap around the handle since they need to be inserted into the thimbles. Holding the device with 3 fingers only might be causing a higher pressure to be exerted in the lower half of the palm.

Chapter 6

CONCLUSION

We have developed a compact handheld haptic device capable of displaying force and stretch feedback to the user. We investigated the effect of visual cues on the haptic perception of object stiffness using the force feedback feature of the device. We also quantified the stretch feedback displayed by the device inside the user's palm.

The results of our force feedback experiments show that humans rely on visual information more in stiffness discrimination when there is a conflict between visual and haptic cues displayed to them. More generally, all the previous observations on the visual and haptic perception of geometric properties of objects such as size, shape, and orientation and the results described above on the perception of material property, the stiffness (or, equivalently, its reciprocal, the compliance), lead to the following unified explanation: In perceptual tasks that involve spatial perception where information about forces is not essential to the task, visual information supersedes haptic information. However, when the temporal variation of force, a variable that can only be perceived through touch, is essential to the perceptual task, haptic force information is combined with visual spatial information to arrive at human perceptual judgments. Given that the visual spatial resolution is superior to that of kinesthesia, this selective retention of haptic force information while throwing away the kinesthetic hand positional information is optimal during exploration of our natural environment but can go awry when the environmental rules of engagement are altered.

The results of stretch feedback experiments show that tactor displacement and speed strongly influence the perceived intensity of the skin stretch. The perceived stretch magnitudes were not significantly different between the radial (up) and ulnar (down) directions.

In the future, the following improvements can be made to the device:

- An Inertial Measurement Unit (IMU) can be integrated into the device to simulate inertial haptic effects in virtual environments such as shaking a box filled with items or a bottle filled with liquid.

- Our haptic device can be integrated with a tracking unit (e.g., HTC Vive tracker) to simulate hand position and orientation in virtual environments.

- A wearable unit including the controller board and the battery can be designed and integrated with our haptic device to make it untethered. This wearable unit can be attached to the forearm of the user via a soft touch fastener.

- A VR application combining the device's force and stretch feedback features can be developed to demonstrate its full capability. In order to develop such an application, data-driven haptic models can be constructed by attaching sensors to the physical objects and measuring their stiffness and inertia.

BIBLIOGRAPHY

[Amemiya and Gomi, 2012] Amemiya, T. and Gomi, H. (2012). Directional torque perception with brief, asymmetric net rotation of a flywheel. *IEEE Transactions on Haptics*, 6(3):370–375.

[Arasan et al., 2015] Arasan, A., Basdogan, C., and Sezgin, T. M. (2015). Haptistylus: A novel stylus for conveying movement and rotational torque effects. *IEEE Computer Graphics and Applications*, 36(1):30–41.

[Basdogan et al., 2001] Basdogan, C., Ho, C.-H., and Srinivasan, M. A. (2001). Virtual environments for medical training: graphical and haptic simulation of laparoscopic common bile duct exploration. *IEEE/ASME Transactions On Mechatronics*, 6(3):269–285.

[Benko et al., 2016] Benko, H., Holz, C., Sinclair, M., and Ofek, E. (2016). Normaltouch and texturetouch: High-fidelity 3d haptic shape rendering on handheld virtual reality controllers. In *Proceedings of the 29th Annual Symposium on User Interface Software and Technology*, pages 717–728.

[Bianchi et al., 2016] Bianchi, M., Battaglia, E., Poggiani, M., Ciotti, S., and Bicchi, A. (2016). A wearable fabric-based display for haptic multi-cue delivery. In *2016 IEEE Haptics Symposium (HAPTICS)*, pages 277–283. IEEE.

[Caldiran et al., 2019] Caldiran, O., Tan, H. Z., and Basdogan, C. (2019). Visuohaptic discrimination of viscoelastic materials. *IEEE Transactions on Haptics*, 12(4):438–450.

[Chinello et al., 2017] Chinello, F., Pacchierotti, C., Malvezzi, M., and Prattichizzo, D. (2017). A three revolute-revolute-spherical wearable fingertip cutaneous device for stiffness rendering. *IEEE Transactions on Haptics*, 11(1):39–50.

[Choi et al., 2016] Choi, I., Hawkes, E. W., Christensen, D. L., Ploch, C. J., and Follmer, S. (2016). Wolverine: A wearable haptic interface for grasping in virtual reality. In *2016 IEEE/RSJ International Conference on Intelligent Robots and Systems (IROS)*, pages 986–993. IEEE.

[Choi et al., 2018] Choi, I., Ofek, E., Benko, H., Sinclair, M., and Holz, C. (2018). Claw: A multifunctional handheld haptic controller for grasping, touching, and triggering in virtual reality. In *Proceedings of the 2018 CHI Conference on Human Factors in Computing Systems*, pages 1–13.

[Cividanes and Srinivasan, 2001] Cividanes, A. J. and Srinivasan, M. A. (Feb 2001). Visual and haptic interactions in the perception of stiffness in virtual environments. Technical Report Touch Lab Report 18, RLE-TR 640, MIT The Research Laboratory of Electronics.

[Culbertson et al., 2018] Culbertson, H., Schorr, S. B., and Okamura, A. M. (2018). Haptics: The present and future of artificial touch sensation. *Annual Review of Control, Robotics, and Autonomous Systems*, 1(1):385–409.

[Dangxiao et al., 2019] Dangxiao, W., Yuan, G., Shiyi, L., Zhang, Y., Weiliang, X., and Jing, X. (2019). Haptic display for virtual reality: progress and challenges. *Virtual Reality & Intelligent Hardware*, 1(2):136–162.

[Drewing et al., 2009] Drewing, K., Ramisch, A., and Bayer, F. (2009). Haptic, visual and visuo-haptic softness judgments for objects with deformable surfaces. In *World Haptics 2009-Third Joint EuroHaptics conference and Symposium on Haptic Interfaces for Virtual Environment and Teleoperator Systems*, pages 640–645. IEEE.

[Ernst et al., 2000] Ernst, M. O., Banks, M. S., and Bülthoff, H. H. (2000). Touch can change visual slant perception. *Nature Neuroscience*, 3(1):69–73.

[Flanagan and Lederman, 2001] Flanagan, J. R. and Lederman, S. J. (2001). Feeling bumps and holes. *Nature*, 412(6845):389–391.

[Gleeson et al., 2010] Gleeson, B. T., Horschel, S. K., and Provancher, W. R. (2010). Design of a fingertip-mounted tactile display with tangential skin displacement feedback. *IEEE Transactions on Haptics*, 3(4):297–301.

[Gu et al., 2016] Gu, X., Zhang, Y., Sun, W., Bian, Y., Zhou, D., and Kristensson, P. O. (2016). Dexmo: An inexpensive and lightweight mechanical exoskeleton for motion capture and force feedback in vr. In *Proceedings of the 2016 CHI Conference on Human Factors in Computing Systems*, pages 1991–1995.

[Guzererler et al., 2016] Guzererler, A., Provancher, W. R., and Basdogan, C. (2016). Perception of skin stretch applied to palm: Effects of speed and displacement. In *International Conference on Human Haptic Sensing and Touch Enabled Computer Applications*, pages 180–189. Springer.

[Hinchet et al., 2018] Hinchet, R., Vechev, V., Shea, H., and Hilliges, O. (2018). Dextres: Wearable haptic feedback for grasping in vr via a thin form-factor electrostatic brake. In *Proceedings of the 31st Annual ACM Symposium on User Interface Software and Technology*, pages 901–912.

[InterlinkElectronics, 2018] InterlinkElectronics (2018). *Force Sensing Resistor Integration Guide*.

[Kyung and Lee, 2008] Kyung, K.-U. and Lee, J.-Y. (2008). Ubi-pen: a haptic interface with texture and vibrotactile display. *IEEE Computer Graphics and Applications*, 29(1):56–64.

[Lécuyer et al., 2000] Lécuyer, A., Coquillart, S., Kheddar, A., Richard, P., and Coiffet, P. (2000). Pseudo-haptic feedback: Can isometric input devices simulate force feedback? In *Proceedings IEEE Virtual Reality 2000 (Cat. No. 00CB37048)*, pages 83–90. IEEE.

[Lederman and Abbott, 1981] Lederman, S. J. and Abbott, S. G. (1981). Texture perception: studies of intersensory organization using a discrepancy paradigm,

and visual versus tactual psychophysics. *Journal of Experimental Psychology: Human Perception and Performance*, 7(4):902.

[Minsky, 1995] Minsky, M. D. R. (1995). *Computational haptics: the sandpaper system for synthesizing texture for a force-feedback display*. PhD thesis, Massachusetts Institute of Technology.

[Morgenbesser and Srinivasan, 1996] Morgenbesser, H. B. and Srinivasan, M. A. (1996). Force shading for haptic shape perception. In *ASME DSC*, volume 58, pages 407–412.

[Murray et al., 2003] Murray, A., Klatzky, R., and Khosla, P. (2003). Psychophysical characterization and testbed validation of a wearable vibrotactile glove for telemanipulation. *Presence*, 12:156–182.

[Pacchierotti et al., 2017] Pacchierotti, C., Sinclair, S., Solazzi, M., Frisoli, A., Hayward, V., and Prattichizzo, D. (2017). Wearable haptic systems for the fingertip and the hand: taxonomy, review, and perspectives. *IEEE Transactions on Haptics*, 10(4):580–600.

[Paré et al., 2002] Paré, M., Carnahan, H., and Smith, A. M. (2002). Magnitude estimation of tangential force applied to the fingerpad. *Experimental Brain Research*, 142:342–348.

[Perret and Vander Poorten, 2018] Perret, J. and Vander Poorten, E. (2018). Touching virtual reality: a review of haptic gloves. In *ACTUATOR 2018; 16th International Conference on New Actuators*, pages 1–5. VDE.

[Peterlik et al., 2010] Peterlik, I., Sedef, M., Basdogan, C., and Matyska, L. (2010). Real-time visio-haptic interaction with static soft tissue models having geometric and material nonlinearity. *Computers & Graphics*, 34(1):43–54.

[Robles-De-La-Torre and Hayward, 2001] Robles-De-La-Torre, G. and Hayward, V.

(2001). Force can overcome object geometry in the perception of shape through active touch. *Nature*, 412(6845):445–448.

[Sedef et al., 2006] Sedef, M., Samur, E., and Basdogan, C. (2006). Real-time finite-element simulation of linear viscoelastic tissue behavior based on experimental data. *IEEE Computer Graphics and Applications*, 26(6):58–68.

[Sinclair et al., 2019] Sinclair, M., Ofek, E., Gonzalez-Franco, M., and Holz, C. (2019). Capstancrunch: A haptic vr controller with user-supplied force feedback. In *Proceedings of the 32nd annual ACM symposium on user interface software and technology*, pages 815–829.

[Srinivasan and LaMotte, 1995] Srinivasan, M. A. and LaMotte, R. H. (1995). Tactual discrimination of softness. *Journal of Neurophysiology*, 73(1):88–101.

[Srinivassan et al., 1996] Srinivassan, M., Beauregard, G., and Brock, D. (1996). The impact of visual information on the haptic perception of stiffness in virtual environments. *Proc. ASME Dynamic Systems and Control Div.*, 58:555–559.

[Tan et al., 1992] Tan, H. Z., Pang, X. D., Durlach, N. I., et al. (1992). Manual resolution of length, force, and compliance. *Advances in Robotics*, 42:13–18.

[Tan et al., 1994] Tan, H. Z., Srinivasan, M. A., Eberman, B., and Cheng, B. (1994). Human factors for the design of force-reflecting haptic interfaces. *Dynamic Systems and Control*, 55(1):353–359.

[Tiest and Kappers, 2009] Tiest, W. M. B. and Kappers, A. M. (2009). Cues for haptic perception of compliance. *IEEE Transactions on Haptics*, 2(4):189–199.

[Walker et al., 2019] Walker, J. M., Zemiti, N., Poignet, P., and Okamura, A. M. (2019). Holdable haptic device for 4-dof motion guidance. In *2019 IEEE World Haptics Conference (WHC)*, pages 109–114. IEEE.

[Warren and Rossano, 2013] Warren, D. H. and Rossano, M. J. (2013). Intermodality relations: Vision and touch. In *The Psychology of Touch*, pages 131–150. Psychology Press.

[Welch, 1986] Welch, R. B. (1986). Intersensory interactions. *Handbook of Perception and Human Performance.; Sensory Processes and Perception*.

[Whitmire et al., 2018] Whitmire, E., Benko, H., Holz, C., Ofek, E., and Sinclair, M. (2018). Haptic revolver: Touch, shear, texture, and shape rendering on a reconfigurable virtual reality controller. In *Proceedings of the 2018 CHI Conference on Human Factors in Computing Systems*, pages 1–12.

[Winfree et al., 2009] Winfree, K. N., Gewirtz, J., Mather, T., Fiene, J., and Kuchenbecker, K. J. (2009). A high fidelity ungrounded torque feedback device: The itorqu 2.0. In *World Haptics 2009-Third Joint EuroHaptics conference and Symposium on Haptic Interfaces for Virtual Environment and Teleoperator Systems*, pages 261–266. IEEE.

[Wu et al., 1999] Wu, W.-C., Basdogan, C., and Srinivasan, M. A. (1999). Visual, haptic, and bimodal perception of size and stiffness in virtual environments. In *ASME International Mechanical Engineering Congress and Exposition*, volume 16349, pages 19–26. American Society of Mechanical Engineers.

Appendix A

HAPTIC DEVICE INTERFACE

We have developed a graphical user interface (Fig. A.1) to read and manipulate the parameters of the device.

This interface establishes a serial connection through the specified *Port* with a specific *Baudrate*. After the connection is established, the user can display the incoming signals from the haptic device using the *Animator* button. This application offers a user-friendly interface where the user can select between *Finger* and *Palm* mechanisms by selecting the relevant button in the section of *Haptic Device State*.

Based on the selected mechanism by the user, the interface shows the current conditions of the device in the corresponding columns. These conditions include the encoder's position and velocity, and controller mode and type. The user can also force-stop the device using the ***STOP FINGER/PALM*** buttons shown in the figure.

In the next row of the interface window, there are two columns, which enable the user to select the desired control mode for the device. In the column on the left, namely *Controller Mode*, the user first chooses the motor (*Finger* or *Palm*) to be controlled. Then, the type of controller, including *Position Control*, *Velocity Control*, or *Force Control* is selected. The user could also change the control gains. The other column, namely *Waveform Generator*, defines the controller's desired path. First, the user should again select the correct motor to define the path. Then, the user chooses the type of waveform from a list, including Constant, Square, Sawtooth, Triangle, Sinusoidal, and Trapzoidal. Finally, the user sets the desired amplitude, frequency, and offset for the waveform path to be followed by the controller. The GUI also shows the encoded *Serial* messages and some *Info* messages in the last row of the app.

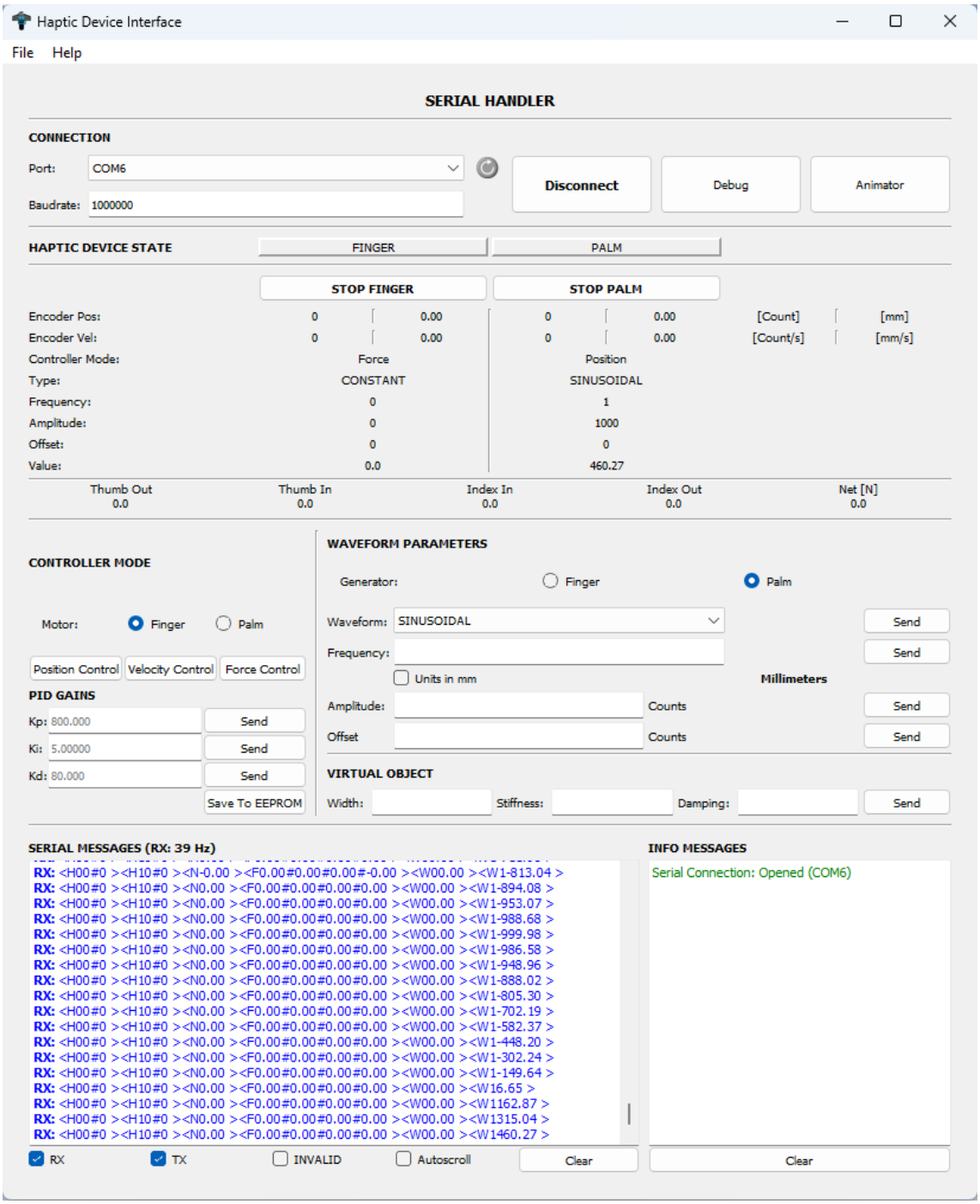

Figure A.1: Haptic device interface provides a graphical user interface to monitor and control the device over the serial port of a personal computer.